Reaction Channel selection techniques and γ – γ fast-timing spectroscopy using the v-Ball Spectrometer

Reaction Channel selection techniques and $\gamma - \gamma$ fast-timing spectroscopy using the ν-Ball Spectrometer

R.L. Canavan[1,2], M. Rudigier[1,3], P.H. Regan[1,2], M. Lebois[4,5], J.N. Wilson[4,5], N. Jovancevic[4,5], P.-A. Söderström[6], D. Thisse[4,5], J. Benito[7], S. Bottoni[8], M. Brunet[1], N. Cieplicka-Oryńczak[9], S.M. Collins[1,2], S. Courtin[10], D.T. Doherty[1], L.M. Fraile[7], K. Hadyńska-Klęk[1,11], M. Heine[10], Ł.W. Iskra[8,9], V. Karayonchev[12], A. Kennington[1], P. Koseoglou[3,13], G. Lotay[1], G. Lorusso[2], M. Nakhostin[1], C.R. Niţă[14], S. Oberstedt[15], Zs. Podolyák[1], L. Qi[4,5], J.-M. Régis[12], R. Shearman[2], V. Vedia[7], W. Witt[3,13]

[1] Department of Physics, University of Surrey, Guildford, GU2 7XH, UK
[2] National Physical Laboratory, Teddington, Middlesex, TW11 0LW, UK
[3] Institut für Kernphysik, Technische Universität Darmstadt, Schlossgartenstrasse 9, 64289, Darmstadt, Germany
[4] IPN Orsay, Paris, France
[5] Université Paris-Saclay, 15 Rue G. Clémenceau, 91406 Orsay Cedex, France
[6] Extreme Light Infrastructure - Nuclear Physics (ELI-NP), Strada Reactorului 30, Măgurele 077126, Romania
[7] Grupo de Física Nuclear & IPARCOS, Universidad Complutense de Madrid, CEI Moncloa, 28040 Madrid, Spain
[8] Dipartimento di Fisica, Universitá degli Studi di Milano and INFN sez. Milano, I-20133, Milano, Italy
[9] Institute of Nuclear Physics, Polish Academy of Sciences, PL-31-342 Kraków, Poland
[10] IPHC and CNRS, Université de Strasbourg, F-67037 Strasbourg, France
[11] Faculty of Physics, University of Warsaw, PL 02-093, Warsaw, Poland
[12] Institut für Kernphysik der Universität zu Köln, Zülpicher Strasse 77, D-50937 Köln, Germany
[13] GSI Helmholtzzentrum für Schwerionenforschung GmbH, 64291 Darmstadt, Germany
[14] Horia Hulubei National Institute of Physics and Nuclear Engineering (IFIN-HH), R-077125 Bucharest, Romania
[15] European Commission, Joint Research Centre, Directorate G, Retieseweg 111, 2440 Geel, Belgium

E-mail: r.canavan@surrey.ac.uk

Abstract. The reaction of a pulsed ^{18}O beam on a self-supporting and gold-backed isotopically-enriched ^{164}Dy target of thickness 6.3 mg/cm^2 at separate primary beam energies of 71, 76 and 80 MeV was studied at the accelerator at the ALTO facility of the IPN Orsay. The γ rays produced were detected using the newly-constructed ν-Ball spectrometer which comprised of HPGe and $LaBr_3$(Ce) detectors. This conference paper describes the methodology and effectiveness of multiplicity/sum-energy gating, for channel selection between fusion evaporation events and lower multiplicity/energy events from inelastic nuclear scattering and Coulomb excitation of the target, and from two-neutron transfer reactions to ^{166}Dy.

1. Introduction

The ν-Ball array at IPN Orsay is a hybrid HPGe-$LaBr_3$ coincident γ-ray spectrometer [1, 2, 3] comprising 24 HPGe Clover detectors, 10 Phase-I coaxial HPGe detectors, and 20 $LaBr_3$(Ce) (from here on referred to as $LaBr_3$) scintillator detectors supplied by the FATIMA collaboration. All of the HPGe detectors were shielded against Compton scattering using BGO scintillators. This detector combination took advantage of both the excellent energy resolution of the HPGe detectors, and the excellent timing resolution of the $LaBr_3$ scintillator detectors. The BGO detectors could also be used for enhanced calorimetry measurements to help with event selection, since they were not shielded from the target position in this configuration.

The first in-beam experiment with ν-Ball took place in November 2017. A pulsed ^{18}O beam impinged on a ^{164}Dy target (6.3 mg/cm^2 enriched ^{164}Dy, 1 mg/cm^2 Au backing). The primary beam was provided at three separate energies, 71, 76, and 80 MeV, which were run for ∼22, ∼60 and ∼48 hours respectively. At each energy the beam was pulsed, with a duration of 2 ns and a period of 400 ns, and an average current of ∼35 enA in charge state $Q = 6^+$. The data were acquired with a trigger in place, so events were accepted when at least one $LaBr_3$ and one HPGe, or, two $LaBr_3$ detectors were hit within 2 μs. The desired reaction was via ^{164}Dy(^{18}O,^{16}O)^{166}Dy. The production of this channel was significantly suppressed relative to the main reaction channels (with cross sections approximately 10^3 times larger than the 2n transfer) from the Coulomb excitation/inelastic scattering on the ^{164}Dy target nucleus, and the ^{164}Dy(^{18}O,4n)^{178}W fusion evaporation reaction. In this contribution, the ability to separate out the ^{164}Dy, ^{166}Dy and ^{178}W nuclei produced, using HPGe energy coincidence gating and the effects of fold-sum energy conditions, will be presented. Details on the lifetime analyses of the data from this experiment have been submitted by M. Rudigier et. al to Phys. Lett. B (for ^{178}W analyses) and by R.L. Canavan et. al. to Phys. Rev. C (for ^{164,6}Dy analyses).

2. Examples and Results of Reaction Channel Selection using ν-Ball

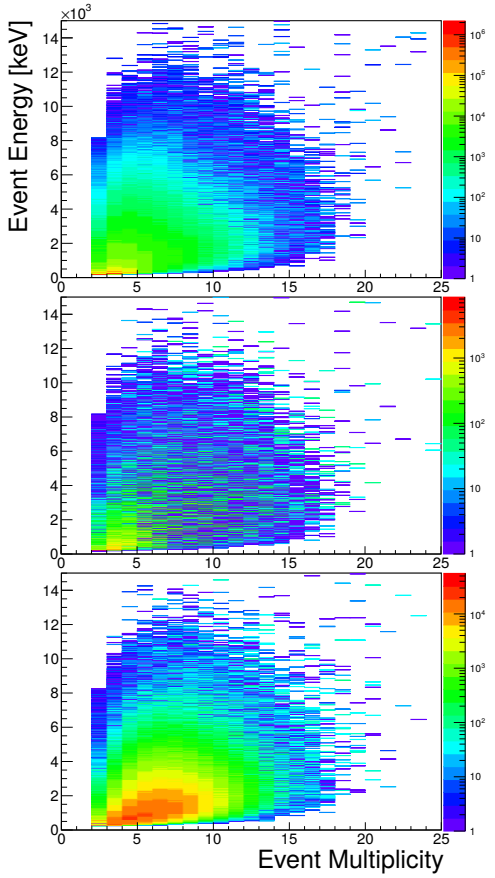

Figure 1. *[COLOR ONLINE] Total event energy vs. total event multiplicity distributions for events which populate excited states in* ^{164}Dy, ^{166}Dy and ^{178}W*, from top to bottom. Background-subtracted HPGe gates were set at 169, 177 and 237 keV to produce the top, middle and bottom plots respectively. These events contained a minimum of two HPGe detectors firing and use data which were taken at a beam energy of 71 MeV.*

Event total energy and multiplicity (number of detectors fired) was used to improve the channel selection capabilities in the current work. The three main reaction nuclei, ^{164}Dy, ^{166}Dy and ^{178}W, are produced via different reaction mechanisms, each of which has its own distribution of total event energy (E) and total event multiplicity (N). Where $E = E(nHPGe) + E(nLaBr_3) + E(nBGO)$ and $N = nHPGe + nLaBr_3 + nBGO$; and where $nHPGe$ is the HPGe detector multiplicity after add-back and Compton suppression, $nLaBr_3$ is the $LaBr_3$ detector multiplicity, and $nBGO$ is the BGO multiplicity in events which were not Compton vetoed. The gamma rays which contribute to the event energy and multiplicity are those which have not been Compton vetoed, and which are detected within the 2 μs coincidence window of each event.

Figure 1 shows the distribution of E vs. N, for the three main reaction channels in the current work, to produce ^{164}Dy, ^{166}Dy or ^{178}W. The matrices use events which have at least two prompt HPGe detections (within 50 ns of the beam pulse), from data taken with a beam energy of 71 MeV. A HPGe energy gate was set on the $4^+ \rightarrow 2^+$ transition in either ^{164}Dy, ^{166}Dy or ^{178}W, at 169, 177 and 237 keV, respectively [4, 5, 6] (see total projections in Fig. 3), to select the desired nucleus; a background subtraction was also made for each matrix. The projections from the matrices shown in Figure 1 are shown in Figure 2.

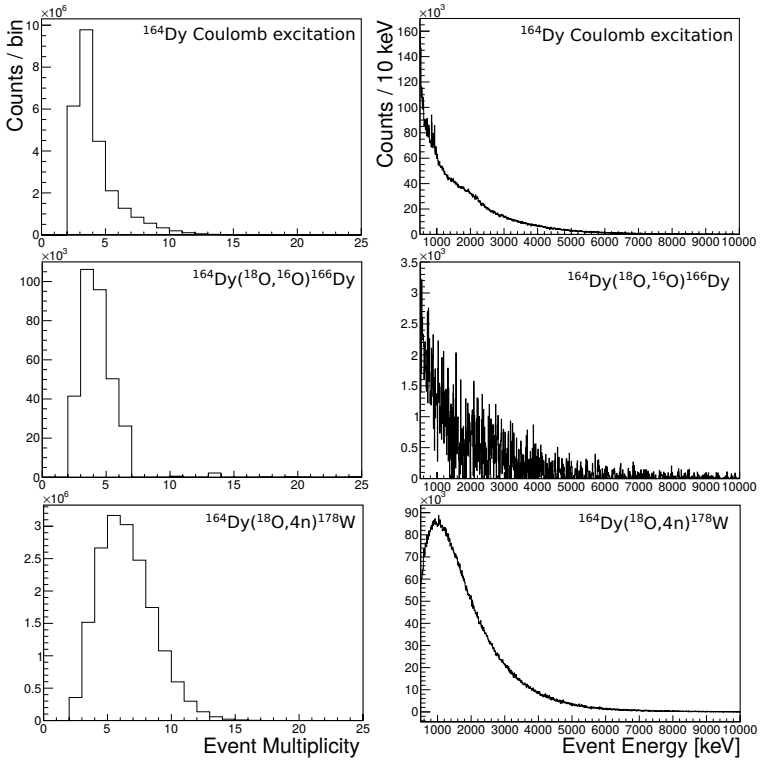

Figure 2. *Projections of the total event energy and total event multiplicity distributions for events which populate excited states in* ^{164}Dy, ^{166}Dy and ^{178}W*, from top to bottom. Background-subtracted HPGe gates were set at 169, 177 and 237 keV to produced the top, middle and bottom plots respectively. These data were taken at a beam energy of 71 MeV.*

Figure 3 shows the ability to separate out the Coulomb excitation and inelastic target excitation from the fusion evaporation reaction channels using constraints on E and N. HPGe-HPGe matrices were created with the constraint that at least two HPGe detectors fired within 50 ns of the beam pulse, within the 2 μs event window. Additional constraints were placed on some of the matrices to preferentially select either fusion evaporation or Coulomb excitation events. The upper plot gives the projection of the prompt HPGe-HPGe matrix, with no additional constraints, at 71 MeV beam energy. The central plot has $N \geq 4$ and $E > 2$ MeV constraints to select transitions originating from ^{178}W. The lower plot has $2 \leq N \leq 3$ and $E < 2$ MeV constraints to pick out transitions originating from ^{164}Dy.

This technique for selecting γ rays from a particular nucleus allows double-coincident events to be used (e.g. HPGe-HPGe) rather than triple-coincident events which have significantly lower statistics. Coulomb excitation and fusion evaporation events are easily separated because of the different ways in which excited states are populated. For Coulomb excitation, the reaction does not transfer much angular momentum, so only states with low spin are populated and not many γ rays are emitted; these events have a low total energy emittance and low γ-ray multiplicity. For fusion evaporation, the reaction transfers a lot of angular momentum, states which are high up the yrast band are populated producing a large cascade of γ rays; these events have a high total energy emittance and high γ-ray multiplicity.

In the current work the fusion evaporation reaction ^{164}Dy(^{18}O,3n)^{179}W also took place, so γ rays depopulating excited states in ^{179}W were seen. By gating on the $11/2^- \rightarrow 7/2^-$ transition at 265 keV in ^{179}W, and applying a background subtraction, the total event energy and total event multiplicity distribution could be plotted for this fusion evaporation reaction channel. Figure 4 compares the total event energy and multiplicity distributions for the two fusion evaporation

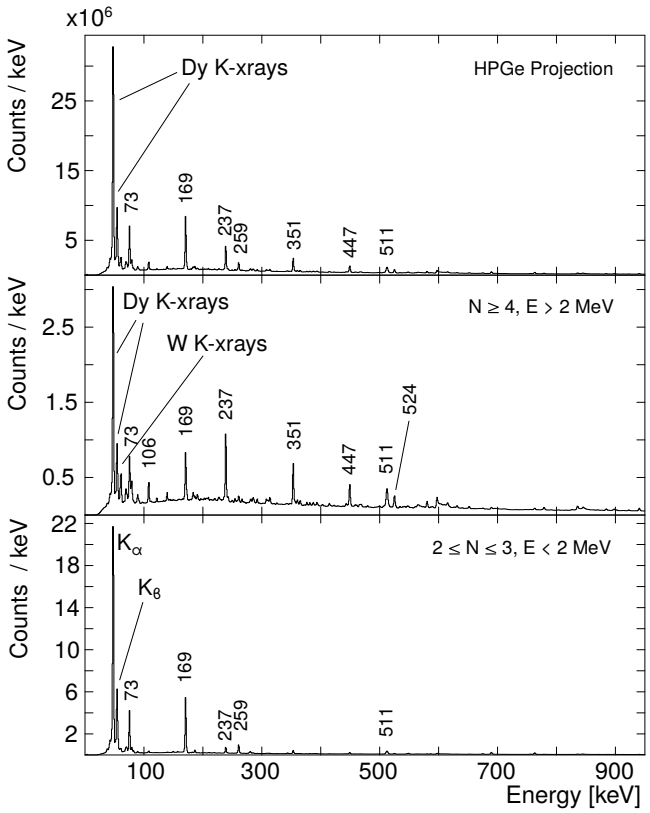

Figure 3. *(Top) Projection of prompt HPGe-HPGe coincidence matrix, with a coincidence time window of ± 50 ns around the prompt beam pulse. (Middle) Projection of prompt HPGe-HPGe matrix with $N \geq 4$ and $E > 2$ MeV. (Bottom) Projection of prompt HPGe-HPGe matrix with $2 \leq N \leq 3$ and $E < 2$ MeV. These data were taken at a beam energy of 71 MeV.*

reaction channels in the current work. The events used contained at least two HPGe detections within 50 ns of the beam pulse, for a beam energy of 71 MeV. Despite the low statistics for the weaker ^{164}Dy(^{18}O,3n)^{179}W channel, there is a clear difference in the shapes of the total event energy and multiplicity distributions for the two types of fusion evaporation.

Due to the relatively low cross section for the ^{166}Dy nucleus excitation, compared to that of ^{164}Dy and ^{178}W, it was difficult to separate out the γ rays from ^{166}Dy using only E and N conditions. However, by using E and N constraints in combination with a HPGe energy gate on a transition in ^{166}Dy, the γ rays emitted by this nucleus could be seen clearly.

Figure 5 demonstrates the ability to separate the ^{164}Dy and ^{166}Dy nuclei using background-subtracted HPGe energy gates. The plots are created from a prompt HPGe-HPGe coincidence matrix using the data taken at 71 MeV beam energy; where at least two HPGe detectors fired within 50 ns of the beam pulse and the 2 μs event window contained $N \leq 4$. The upper plot shows the HPGe spectrum after gating on the yrast $4^+ \rightarrow 2^+$ transition at 169 keV in ^{164}Dy and applying a background subtraction. The upper-middle plot shows the HPGe spectrum after gating on the yrast $4^+ \rightarrow 2^+$ transition at 177 keV in ^{166}Dy and applying a background subtraction. The lower-middle plot shows the HPGe spectrum after gating on the $(2^+) \rightarrow 0^+_{g.s}$ transition at 857 keV in ^{166}Dy and applying a background subtraction. The lower plot shows the HPGe spectrum after gating on the $(4^-) \rightarrow (3^+)$ transition at 252 keV in ^{166}Dy and applying a background subtraction. All background subtractions were performed by subtracting a background-gated HPGe projection from the peak-gated HPGe projection, using the 237 keV peak for the normalisation factor. The difference in cross section of the Coulomb excitation and

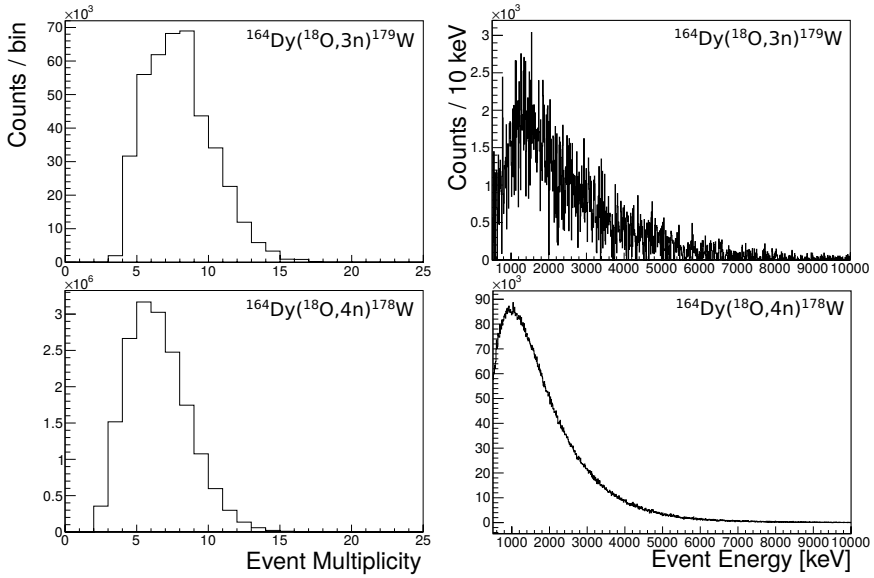

Figure 4. *Projections of the total event energy and total event multiplicity distributions for events which populate excited states in ^{178}W and ^{179}W. The upper plots show the event energy and multiplicity distributions for the 3n fusion evaporation reaction channel to ^{179}W, while the lower plots show the event energy and multiplicity distributions for the 4n fusion evaporation reaction channel to ^{178}W. The HPGe energy gates used to select the ^{178}W and ^{179}W nuclei were 237 keV ($4^+ \rightarrow 2^+$ transition in ^{178}W) and 265 keV ($11/2^- \rightarrow 7/2^-$ transition in ^{179}W) respectively [6, 7]. These data were taken at a beam energy of 71 MeV.*

2n transfer reactions is clear from the reduction in gamma rays originating from ^{166}Dy. However, the peaks are clear enough to verify which excited states were populated in ^{166}Dy during the 2n transfer reaction.

From this channel selection it was then possible to make HPGe-gated LaB_3 E-E-Δ T cubes for obtaining lifetime measurements in either ^{164}Dy, ^{166}Dy or ^{178}W, by setting energy gates on a feeder and decay transition and measuring the mean time difference between them.

3. Conclusion

The capabilities of the ν-Ball array for reaction channel selection have been demonstrated using the data from the first NuBall campaign in November 2017. Using a HPGe energy gate on the $4^+ \rightarrow 2^+$ transition in the ^{164}Dy, ^{166}Dy, ^{178}W and ^{179}W nuclei, it was possible to see the different patterns of total event energy (E) and total event multiplicity (N) for different reaction types. By setting conditions on E and N it was possible to separate out the γ rays produced by Coulomb excitation and fusion evaporation reactions, from the ^{164}Dy and ^{178}W nuclei respectively. Using a combination of E and N conditions and background subtracted HPGe gates it was possible to separate out the gamma rays emitted by ^{164}Dy and ^{166}Dy for fast-timing analyses. All figures were made using data collected at the 71 MeV beam energy as an example. At this (lowest) beam energy the conditions were the most suitable for Coulomb excitation reactions, which gave a good mixture of gamma rays from the different reaction types. Therefore, the 71 MeV beam energy dataset was the best one to show the effectiveness of the reaction channel selection techniques.

Acknowledgments

The authors would like to thank the operators of the ALTO facility for providing the reliable beams used during the experiment. Additionally we thank the FASTER collaboration for the technical support given. GAMMA-POOL and LOANPOOL are acknowledged for loaning the

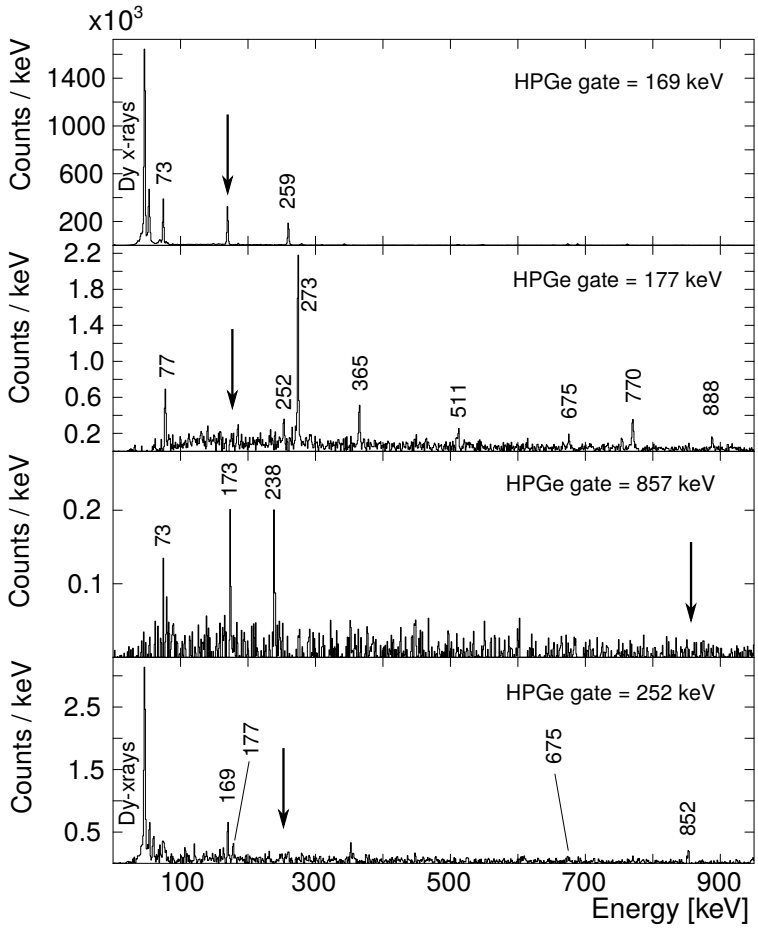

Figure 5. *Background-subtracted gated projections from a prompt HPGe-HPGe coincidence matrix, with $N \leq 4$ for the 2 μs event, after gating on the 169 keV $4^+ \rightarrow 2^+$ transition in ^{164}Dy, and the 177 keV $4^+ \rightarrow 2^+$ transition, the 857 keV $2_2^+ \rightarrow 0^+$ transition and the 252 keV $(4^-) \rightarrow (3^+)$ transition in ^{166}Dy respectively. Arrows indicate the energies where gates were set. These data were taken at a beam energy of 71 MeV.*

Clover and Phase I HPGe detectors. The FATIMA collaboration is acknowledged for loaning the LaB_3 detectors. This work was supported by the STFC UK Nuclear Data Network, the STFC (grant numbers ST/L005743/1 and ST/P005314), the Marion Redfearn Trust, BMBF (NUSTAR.DA grant No. 05P15RDFN1), and Spanish MINECO grant FPA2015-65035-P. The research leading to these results has received funding from the European Union's HORIZON2020 Program under grant agreement no. 654002. P.H.R. and S.M.C. acknowledges support from the UK Department of Business, Energy and Industrial Strategy (BEIS) via the National Measurement System.

References

[1] Lebois M et. al. 2019 *Acta Physica Polonica B* **50** 425
[2] Jovančević N et. al. 2019 *Acta Physica Polonica B* **50** 297
[3] Rudigier M et. al. 2019 *Acta Physica Polonica B* **50** 661
[4] Singh B et. al. 2018 *Nuclear Data Sheets* **147** 1-381
[5] Baglin C.M et. al. 2008 *Nuclear Data Sheets* **109** 1103-1382
[6] Achterberg E et. al. 2009 *Nuclear Data Sheets* **110** 1473-1688
[7] Baglin C.M et. al. 2009 *Nuclear Data Sheets* **110** 265-506